



## Research paper

# Dysregulated bile acid signaling contributes to the neurological impairment in murine models of acute and chronic liver failure



Guoxiang Xie<sup>a,b,1</sup>, Xiaoning Wang<sup>c,d,1</sup>, Runqiu Jiang<sup>b,e,1</sup>, Aihua Zhao<sup>a</sup>, Jingyu Yan<sup>c</sup>, Xiaojiao Zheng<sup>a</sup>, Fengjie Huang<sup>a</sup>, Xinzhu Liu<sup>c</sup>, Jun Panee<sup>f</sup>, Cynthia Rajani<sup>b</sup>, Chun Yao<sup>g</sup>, Herbert Yu<sup>b</sup>, Weiping Jia<sup>a</sup>, Beicheng Sun<sup>e</sup>, Ping Liu<sup>c,d,\*\*</sup>, Wei Jia<sup>a,b,\*</sup>

<sup>a</sup> Shanghai Key Laboratory of Diabetes Mellitus and Center for Translational Medicine, Shanghai Jiao Tong University Affiliated Sixth People's Hospital, Shanghai 200233, China

<sup>b</sup> University of Hawaii Cancer Center, Honolulu, HI 96813, USA

<sup>c</sup> E-institute of Shanghai Municipal Education Committee, Institute of Interdisciplinary Integrative Medicine Research, Shanghai University of Traditional Chinese Medicine, Shanghai 201203, China

<sup>d</sup> Key Laboratory of Liver and Kidney Diseases (Ministry of Education), Institute of Liver Diseases, Shuguang Hospital, Shanghai University of Traditional Chinese Medicine, Shanghai 201203, China

<sup>e</sup> Liver Transplantation Center of the First Affiliated Hospital, State Key Laboratory of Reproductive Medicine, Nanjing Medical University, Nanjing, Jiangsu 210029, China

<sup>f</sup> Department of Cell and Molecular Biology, John A. Burns School of Medicine, University of Hawaii at Manoa, Honolulu, HI 96813, USA

<sup>g</sup> Guangxi University of Chinese Medicine, Nanning, Guangxi 530001, China

## ARTICLE INFO

## Article history:

Received 5 June 2018

Received in revised form 4 October 2018

Accepted 10 October 2018

Available online 19 October 2018

## Keywords:

Bile acids

Ammonia

Hepatic encephalopathy

Apical sodium-dependent bile acid transporter

## ABSTRACT

**Background:** Hepatic encephalopathy (HE), a severe neuropsychiatric complication, is associated with increased blood levels of ammonia and bile acids (BAs). We sought to determine (1) whether abnormally increased blood BAs in liver cirrhotic patients with HE is caused by elevation of apical sodium-dependent BA transporter (ASBT)-mediated BA reabsorption; and (2) whether increased BA reabsorption would exacerbate ammonia-induced brain injuries.

**Methods:** We quantitatively measured blood BA and ammonia levels in liver cirrhosis patients with or without HE and healthy controls. We characterized ASBT expression, BA profiles, and ammonia concentrations in a chronic liver disease (CLD) mouse model induced by streptozotocin-high fat diet (STZ-HFD) and an azoxymethane (AOM) - induced acute liver failure (ALF) mouse model. These two mouse models were treated with SC-435 (ASBT inhibitor) and budesonide (ASBT activator), respectively.

**Findings:** Blood concentrations of ammonia and conjugated BAs were substantially increased in cirrhotic patients with HE ( $n = 75$ ) compared to cirrhotic patients without HE ( $n = 126$ ). Pharmacological inhibition of the enterohepatic BA circulation using a luminal- restricted ASBT inhibitor, SC-435, in mice with AOM-induced ALF and STZ-HFD-induced CLD effectively reduced BA and ammonia concentrations in the blood and brain, and alleviated liver and brain damages. Budesonide treatment induced liver and brain damages in normal mice, and exacerbated these damages in AOM-treated mice.

**Interpretation:** ASBT mediated BA reabsorption increases intestinal luminal pH and facilitates conversion of intestinal ammonium to ammonia, leading to abnormally high levels of neurotoxic ammonia and cytotoxic BAs in the blood and brain. Inhibition of intestinal ASBT with SC-435 can effectively remove neurotoxic BAs and ammonia from the bloodstream and thus, mitigate liver and brain injuries resulting from liver failure.

© 2018 The Authors. Published by Elsevier B.V. This is an open access article under the CC BY-NC-ND license (<http://creativecommons.org/licenses/by-nc-nd/4.0/>).

## 1. Introduction

Hepatic encephalopathy (HE) is a constellation of common and potentially severe neuropsychiatric abnormalities present in acute and chronic liver diseases [1]. Blood ammonia is predominantly derived from the intestine and readily crosses the blood-brain barrier (BBB). Accumulation of blood ammonia is believed to play a crucial role in HE pathogenesis [2]. However, recent research has shown that elevated serum bile acids (BAs) are closely associated with liver cirrhosis, hepatocellular carcinoma [3–5], and neurological decline in acute liver failure

\* Correspondence to: W. Jia, University of Hawaii Cancer Center, Honolulu, HI 96813, USA.

\*\* Correspondence to: P. Liu, Institute of Liver Diseases, Shuguang Hospital, Shanghai University of Traditional Chinese Medicine, 528 Zhangheng Road, Shanghai 201203, China.

E-mail addresses: [liuliver@vip.sina.com](mailto:liuliver@vip.sina.com) (P. Liu), [wjia@cc.hawaii.edu](mailto:wjia@cc.hawaii.edu) (W. Jia).

<sup>1</sup> These authors contributed equally to this work.

## Research in context

### Evidence before this study

Hepatic encephalopathy (HE) is a constellation of common and potentially severe neuropsychiatric abnormalities present in acute and chronic liver diseases, affecting 30–50% of patients with liver cirrhosis. Accumulation of ammonia in the blood, which is predominantly derived from the intestine and readily crosses the blood-brain barrier, is believed to play a crucial role in HE pathogenesis. Serum bile acids (BAs) are significantly increased after liver damage, which may disrupt the blood-brain barrier and cause brain damage.

### Added value of this study

Conjugated BAs were significantly elevated in sera of liver cirrhosis patients, and further elevated in those with HE. Apical sodium-dependent bile acid transporter (ASBT) gene expression in ileum and brain and BA concentrations in blood, liver, and brain were significantly increased in a chronic liver disease mouse model induced by streptozotocin-high fat diet (STZ-HFD) as well as an azoxymethane (AOM)-induced acute liver failure mouse model. ASBT mediated BA reabsorption increased pH in the ileum, which facilitated conversion of intestinal ammonium to ammonia, and led to abnormally high levels of cytotoxic BAs and neurotoxic ammonia in blood and brain. Inhibition of the intestinal ASBT with SC-435 in mice effectively reduced BA and ammonia concentrations in the blood and brain, resulting in significant alleviation of liver and brain damages. Administration of ASBT activator, budesonide, induced liver and brain damages in normal mice, and exacerbated these damages in AOM-treated mice.

### Implications of all the available evidence

Enhanced BA reabsorption contributes to the development of HE and may also be a causal factor for other neurodegenerative diseases involving dysregulated BA and ammonia metabolism. Blocking BA reabsorption from the intestine via inhibiting ASBT decreased concentrations of BAs and ammonia in blood and brain in mice with liver failure, ameliorated the development of HE in these mice. Thus, targeting ASBT may become a novel therapeutic approach for chronic neurological conditions that often exhibit impaired BA and ammonia regulation.

(ALF) [6]. A previous report on BA levels in the sera, cerebrospinal fluid, and brain tissue of 10 patients immediately after death from fulminant hepatic disease also indicated that increased serum BAs would lead to an increase in brain BAs during HE [7]. BAs are produced in the liver from cholesterol primarily via the enzyme cytochrome *p*450 7A1, and are then conjugated with glycine or taurine, secreted into the intrahepatic bile capillaries via a bile salt export pump and then exported to the intestine where they are metabolized by microbiota [8]. In the terminal ileum and colon, BAs are reabsorbed by enterocytes via apical sodium-dependent bile acid transporters (ASBT) and then released into the portal vein via two organic solute transporters, OST- $\alpha/\beta$ . In humans, 90–95% of BAs are recycled, and ~75% of which are mediated by the ASBT [9]. ASBT is most highly expressed in the ileum but it has also been detected in the cecum, kidney [10] and duodenum [11]. Ileal BAs are recycled back to the liver where they are taken up primarily by the sodium-dependent taurocholate cotransporting polypeptide (NTCP) [12]. In addition to the enterohepatic circulation, BAs have recently been

reported to distribute to multiple organs including the brain, particularly, in rodents [13,14]. Under healthy conditions, only small amount of BAs are found in the peripheral circulation. However, during liver damage, BAs (especially those conjugated with glycine and taurine) accumulate in the circulation due to increased BA reabsorption from the intestine into the portal vein, and the increased backflux rate of BAs from the hepatocytes into blood [15]. Accumulation of BAs in the circulation may contribute to the development of HE [7,16], however, the underlying mechanisms remain unclear.

The nuclear receptor farnesoid X receptor (FXR; gene symbol *NRIH4*) is the primary hepatic BA sensor studied most extensively for its regulation of numerous genes involved in BA homeostasis [14]. Previous studies have also indicated that FXR may contribute to the homeostasis of multiple neurotransmitter systems in different brain regions and modulate neurobehavior [17]. BAs in the serum have also been shown to gain access to the brain and contribute to the neurological decline associated with HE via a mechanism involving FXR activation [6].

We hypothesized that the ASBT would be upregulated in HE patients and lead to increased enterocyte BA reabsorption. As a result, cytotoxic BAs would start to accumulate in the blood and eventually reach abnormally high levels. An increased intestinal luminal pH would result and facilitate the conversion of ammonium ions into neurotoxic ammonia, which readily diffuses into both the bloodstream and brain. Ultimately, the accumulation of both BAs and ammonia in the brain can lead to brain damage and dysfunction. To test these hypotheses, we analyzed serum BA profiles in newly diagnosed patients with liver cirrhosis with or without HE and healthy controls using a targeted metabolomics approach. We also measured ASBT and NTCP expression as well as BA and ammonia concentrations in different tissues in AOM-induced ALF model mice [18,19]. Different tissue concentrations of BA and ammonia along with ASBT and NTCP protein expression were analyzed in mice with nonalcoholic steatohepatitis (NASH) induced by streptozotocin and high fat diet (STZ-HFD), a model that mimics human liver disease progression from steatosis to NASH, fibrosis, and hepatocellular carcinoma (HCC) [4,20]. The AOM-induced ALF mouse model was also used to test the effects of ASBT agonists and antagonists on HE progression. A small molecule, ASBT inhibitor SC-435 [21], and budesonide [22,23], a potent glucocorticoid that is well absorbed in the intestine and activates the glucocorticoid receptor which is known to upregulate ASBT expression, were used to block or increase BA reuptake in the distal ileum, respectively.

## 2. Materials and methods

### 2.1. Human subjects

A total of 201 liver cirrhosis patients (75 with HE and 126 without HE), aged 15–75 years, were recruited from April 2013 to December 2013 and from December 2014 to June 2015 at two study sites (Shuguang Hospital Affiliated to Shanghai University of Traditional Chinese Medicine, Shanghai, China and the Xiamen Hospital of Traditional Chinese Medicine, Xiamen, China). Ninety-three healthy individuals were recruited as controls from the Physical Examination Center of Shuguang Hospital. Details are provided in the Supplementary Information.

The study was approved by the institutional human subjects review board of both participating hospitals. Each participant signed a written consent form for the study.

### 2.2. Blood sample collection

Fasting blood specimens were collected from all subjects and serum samples were obtained and storage at  $-80^{\circ}\text{C}$  until analysis.

### 2.3. Blood test

Complete blood counts were measured using a COULTER LH750 Hematology Analyzer (USA), coagulation functions were measured with an automatic coagulation analyzer (STAGO Compact, Diagnostica Stago, France), and other biochemical tests were measured using the Beckman Coulter Synchron DXC800 Chemistry Analyzer (USA).

### 2.4. Animal experimentation

Male C57BL/6J mice (25 to 30 g; Vital River Laboratory Animal Technology Co. Ltd., Beijing, China) were used in the experiments with approval from Shanghai University of Traditional Chinese Medicine Institutional Animal Care and Use Committee.

### 2.5. STZ-HFD-induced NASH-HCC C57BL/6J mouse model

New born male C57BL/6J mice were randomly divided into three groups and treated as the following: (1) normal control mice were housed without any treatment and fed normal diet (12 kcal% fat); (2) NASH-HCC mice had a single subcutaneous injection of 200 µg STZ (Sigma, MO, USA) 2 days after birth and were fed with HFD (60 kcal% fat) ad libitum after 4 weeks of age for 16 weeks to induce the HCC [4,20]; and (3) NASH-HCC-SC-435 group, were supplemented with SC-435 (ASBT inhibitor, 10 µg/g body weight, provided by Pfizer, Peapack, NJ) after 4 weeks of age for 16 weeks. The body weight of all animals was measured once a week. At weeks 6, 8, 12 and 20 of age, eight ( $n = 8$ ) mice in each group were euthanized, and their livers and brains were removed and stored at  $-80^{\circ}\text{C}$  for hematoxylin-eosin (H&E) staining. Ileum tissue and content were also collected and stored at  $-80^{\circ}\text{C}$  for future analysis of BAs and gene expression of BA transporters.

### 2.6. AOM-induced HE C57BL/6J mouse model

Male mice were fed ad libitum with normal rodent chow with free access to water. At age week 8, male mice were randomly separated into four groups ( $n = 8$  per group) and treated as the following: (1) control group received a single intraperitoneal injection of 100 µL saline; (2) AOM group received a single intraperitoneal injection of azoxymethane (AOM, 100 µg/g of body weight; Sigma, St. Louis, CO) dissolved in 100 µL saline; (3) AOM/budesonide group were supplemented with budesonide (ASBT activator, 40 µg/g body weight, Sigma) through diet for 5 days before the injection of AOM; and (4) AOM/SC-435 group were supplemented with SC-435 (ASBT inhibitor, 10 µg/g, provided by Pfizer, Peapack, NJ) for 5 days before the injection of AOM. After injection, mice were placed on heating pads set to  $37^{\circ}\text{C}$  to ensure they remained normothermic. After 8 h, mice were provided with 1% glucose ad libitum instead of water to ensure euglycemia and hydration. Glucose solution and rodent chow were placed on cage floors to ensure easy access to food and hydration. Mice were sacrificed at 35 h after the AOM injection [24]. The body weight of all animals was measured and recorded. Organs including liver and brain were removed and stored at  $-80^{\circ}\text{C}$  for histological and immunochemical analysis. In addition, 15 mice in each group were maintained for investigation of survival during the experimental period.

### 2.7. Budesonide treatment in C57BL/6J mice

To test if enhanced BA reabsorption can induce a significant increase of serum and brain ammonia levels, budesonide (40 mg/kg) was administered to adult male C57BL/6J mice through diet for 1 week, and mice on normal chow without budesonide supplement were used as control. Sixteen (16) mice were included in each group. Mice were sacrificed after the 1-week budesonide treatment and perfused with phosphate-buffered saline (PBS) before sample collection. Plasma, liver, brain and

small intestinal tissues and contents were collected and stored at  $-80^{\circ}\text{C}$  for further analyses.

### 2.8. Elevated plus maze neurobehavioral study

An elevated plus maze (RD1104-RM, Mobile Datum Information Technology, Shanghai, China) was used to assess level of anxiety in mice. The elevated plus maze consists of four arms (two closed arms and two open arms) elevated 100 cm above the floor. Anxiety-related behavior is associated with avoidance of the open arms and preference of the closed arms of the maze [25]. Each mouse was placed in the center of the maze and the amount of time spent in each arm was recorded.

### 2.9. Histology, immunohistochemistry and immunofluorescence studies

Liver and brain tissues were fixed in 10% neutral-buffered formalin, embedded in paraffin blocks, and processed for routine H&E staining. The stained sections were subsequently examined for histopathological changes.

For brain immunohistochemistry, brain sections were deparaffinized and then subjected to rehydration steps through a graded ethanol series ending in distilled water. Samples were then treated with 3%  $\text{H}_2\text{O}_2$  in methanol for 30 min to block the endogenous peroxidase activity. The sections were rinsed in PBS twice, 5 min each time and incubated with 10% normal goat serum for 30 min to block non-specific antibody binding. Immunoreactivity was assessed using specific antibodies for GFAP (Cell Signaling, Danvers, MA), and the neuronal marker NeuN (Abcam, San Francisco, CA). After that, the sections were stained with DAB according to manufacturer's protocols and mounted and photographed using a digitalized microscope camera (Nikon, Tokyo, Japan). Positive cells were quantified using Image J software (Media Cybernetics, MD, USA).

For immunofluorescence analysis, brain slides (cerebral cortex) were stained with antibodies for ASBT (Santa Cruz, California, CA), GFAP (Cell Signaling, Danvers, MA), and NeuN (Abcam, San Francisco, CA), followed by staining with Alexa Fluor 488-conjugated anti-mouse IgG (1:500, Ab150117), and Alexa Fluor 555-conjugated anti-rabbit IgG (1:1000, Ab150074) (Abcam, Cambridge, UK) antibodies. The slides were mounted with ProLong® Gold Antifade Mountant (ThermoFisher), and examined using a confocal microscopy (Zeiss, Oberkochen, Germany). Stain-positive cells were quantified using Image J software (Media Cybernetics, MD, USA).

Statistical analyses of percentage of GFAP and NeuN positive cells were independent from each other. For each index, five fields were randomly selected, and the percentage of GFAP+/NeuN+ cells in the cerebral cortex was calculated separately and normalized to the DAPI positive cells. Cerebral cortex is a large brain region and variations in NeuN and GFAP could be a reflection of brain region differences in the density of neurons. To avoid possible sample variability, we then normalized the data in the treatment group to the mean value of the normal control group and showed the results as a fold change. Representative images from the same brain region were used for the analysis.

### 2.10. Liver function marker and ammonia measurements

Plasma ALT and AST were measured using fluorometric activity assays (Sigma-Aldrich), according to the manufacturer's instructions. The ammonia levels were measured using an Ammonia Assay Kit (AA0100, Sigma-Aldrich) according to the manufacturer's protocols.

### 2.11. Quantitative real-time polymerase chain reaction

Total RNA was isolated from liver tissue using TRIzol reagent (Invitrogen, Shanghai, China) according to the manufacturer's protocol. RNA concentration was determined using a GE Nanovue Ultramicro spectrophotometer (Healthcare Bio-Sciences AB, USA). mRNA levels of

the targeted genes were measured in triplicate on a ViiA™ 7 Real-Time PCR System (Invitrogen, Life Technologies,) using a SYBR Green PCR kit. The forward and reverse primers of the target genes were designed and synthesized by Sangon Biotech (Shanghai, China).  $\beta$ -actin was used as a house-keeping gene, and the relative expression of the target genes was calculated using the comparative Ct approach (dCT).

### 2.12. BAs quantitation

BAs in serum, liver, and brain were measured according to previously reported methods [26]. A Waters ACQUITY ultra performance LC system coupled with a Waters XEVO TQ-S mass spectrometer with an ESI source controlled by MassLynx 4.1 software (Waters, Milford, MA) was used for all analyses. Chromatographic separations were performed with an ACQUITY BEH C18 column (1.7  $\mu$ m, 100 mm  $\times$  2.1 mm internal dimensions) (Waters, Milford, MA). UPLC-MS raw data obtained with negative mode were analyzed using TargetLynx applications manager version 4.1 (Waters Corp., Milford, MA) to obtain calibration equations and the quantitative concentration of each BA in the samples.

### 2.13. Cell culture and reagents

Human caecum cell line CCL-251 (NCI-H716) was purchased from ATCC. The cells were maintained in Petri dishes in RPMI 1640 medium (Invitrogen) supplemented with 10% fetal bovine serum (FBS, Gibco, USA) at 37 °C in a 5% CO<sub>2</sub> incubator.

GW4064 and (Z)-Guggulsterone were purchased from Sigma-Aldrich (St. Louis, MO, USA).

### 2.14. 3D co-culture and immunofluorescence staining

CCL-251 cells were cultured in the 3D Petri Dish® system (Micro-Tissues) (RI, USA), a scaffold-free culture system that maximizes cell-to-cell interactions. The cells were treated with different combination of BAs (50  $\mu$ M) for 7 days, washed with PBS and used for immunofluorescence staining.

Micro-tissues were incubated with antibodies including ASBT (ab203205) and FXR (ab187735) purchased from Abcam (Cambridge, MA), followed by incubation with Alexa Fluor 488-conjugated anti-mouse IgG (1:500, Ab150117), Goat anti-Rabbit IgG (H + L), superclonal secondary antibodies Biotin (A27035) and Streptavidin (PE-Cy5.5) (SA1018) (Thermo Fisher Scientific, CA). Results were quantified using Image J software (Media Cybernetics, MD, USA).

### 2.15. Cells treated in 2D culture and Western blot

CLL-251 cells were treated with 15 individual BAs (50  $\mu$ M) including CA, CDCA, TCA, GCA, TCDCA, GCDCA, TLCA, GLCA, TDCA, GDCA, DCA, LCA, UDCA, TUDCA, and GUDCA for 48 h to study the effect of BAs on ASBT expression. The whole cell lysates were prepared as previously described [27]. Boiled samples containing equal amounts of total protein were separated on 10% SDS-PAGE, transferred onto a PVDF membrane and incubated with ASBT (ab203205) and  $\beta$ -actin (ab6276) antibodies (Abcam, Cambridge, MA). The signals were visualized using an ECL kit (Bio-Rad, CA).

### 2.16. Western blot

Brain tissue lysates from the frontal cerebral cortex were obtained, and protein concentrations were determined using a BCA protein assay kit (23,225#, Thermo, California, CA). Western blot analysis was performed as previously described [28]. Equal amounts of protein samples were separated by SDS-PAGE and transferred to NC membranes which were then blocked at room temperature for 1 h in blocking solution. The membranes were then incubated with rabbit monoclonal antibodies against NeuN (ab177487, 1:5000) and rabbit polyclonal

antibodies against GFAP (ab7260, 1:1000) overnight at 4 °C, followed by a 1 h incubation at room temperature with HRP-conjugated goat anti-rabbit secondary antibody. The obtained bands were then scanned and analyzed with the Odyssey quantitative western blot near-infrared system and band density was analyzed using Image J software. GAPDH served as an internal control and experiments were performed in triplicate. All antibodies were purchased from Abcam.

### 2.17. Statistical analysis

The differences between the groups in BAs measurements were analyzed by Student *t*-tests using Holm-Sidak method for multiple comparisons correction using GraphPad Prism 6.0 (GraphPad Software, CA, USA). The difference for survival time was assessed using the log rank test. Survival analysis was performed using GraphPad Prism 6.0. We regarded *p* values of <0.05 as statistically significant. Orthogonal partial least squares-discriminant analysis (OPLS-DA) was performed to discriminate between cirrhosis patients and healthy controls. Scatter plots were drawn using GraphPad Prism 6.0. Correlations between BAs and ammonia were performed using Spearman's correlation analysis.

## 3. Results

### 3.1. Serum BA and ammonia increased significantly in cirrhosis patients

The demographic and clinical characteristics of all newly-diagnosed patients and healthy controls are summarized in Table 1. We observed a clear separation among the healthy controls, cirrhosis patients without HE and cirrhosis patients with HE from an orthogonal partial least squares-discriminant analysis (OPLS-DA) model established with the identified BAs (Fig. 1A, R<sub>2</sub>Y = 0.55, Q<sub>2</sub>Y = 0.547). Consistent with our previous study [3], seventeen BAs were found significantly increased in both groups of cirrhosis patients compared with healthy controls (Table S1 and Fig. 1B). The levels of total BAs, conjugated BAs, glycocholic acid (GCA), glycochenodeoxycholic acid (GCDCA), taurocholic acid (TCA) and taurochenodeoxycholic acid (TCDCA) further increased in patients with HE when compared with patients without HE (Fig. 1C, D). Although the absolute concentration of ursodeoxycholic acid (UDCA) and tauroursodeoxycholic acid (TUDCA) were higher in cirrhosis patients than in controls (Table S1), the proportion of these two BAs in total BAs decreased in patients without HE compared with controls, and further decreased in patients with HE in reference to patients without HE (Fig. 1E). A scatter plot of the blood concentrations of the total BAs against blood concentrations of ammonia is shown in Fig. 1G.

Under the conditions of liver failure, the most important alternative pathway for ammonia detoxification is the formation of glutamine from ammonia and glutamate [29]. The ratio of glutamine to glutamate significantly increased in both groups of cirrhosis patients and further increased in cirrhosis patients with HE compared to those without HE (Fig. S1), suggesting that the HE patients still maintained ammonia detoxification ability. However, serum ammonia levels were further elevated in cirrhosis patients with HE compared to cirrhotic patients without HE, although the group difference was not significant (*p* = .06, Fig. 1F), suggesting that there was increased supply of ammonia to the bloodstream [30], instead of decreased metabolic function of the liver in the HE patients. We further measured serum ammonia levels in carefully selected liver function matched patients with HE (*n* = 11) and without HE (*n* = 11), and as a result, the ammonia levels in the HE patients were significantly higher than patients without HE (Fig. S2).

Correlation analysis also revealed that the serum BA levels significantly (*p* < .05) and positively correlated with serum ammonia levels (Table S2), demonstrating that HE patients with higher serum BA levels also had higher ammonia levels.

**Table 1**  
Demographic and clinical characteristics of study participants.

	Control	Cirrhosis patients	
		Without HE	With HE
Number	n = 93	n = 126	n = 75
Sex (M/F)	70/23	87/39	55/20
Age (years)	48.26 ± 1.23	48.12 ± 1.18	52.18 ± 4.42
BMI (kg/m <sup>2</sup> )	23.6 ± 0.32	22.96 ± 0.32	22.22 ± 0.83
Liver standard tests			
ALT (IU/L)	30.43 ± 1.5	93.51 ± 12.27 <sup>a</sup>	80.32 ± 48.22 <sup>a</sup>
AST (IU/L)	21.65 ± 0.49	72.86 ± 8.41 <sup>a</sup>	98.22 ± 37.45 <sup>a</sup>
TBIL (μmol/L)	14.88 ± 0.49	39.13 ± 4.81 <sup>a</sup>	123.84 ± 29.51 <sup>a,b</sup>
DBIL (μmol/L)	2.18 ± 0.08	10.84 ± 1.72 <sup>a</sup>	45.54 ± 17.08 <sup>a,b</sup>
IBIL (μmol/L)	10.09 ± 0.46	26.97 ± 2.92 <sup>a</sup>	71.71 ± 14.29 <sup>a,b</sup>
ALP (IU/L)	87.52 ± 2.09	118.44 ± 13.05 <sup>a</sup>	169.64 ± 22.15 <sup>a,b</sup>
GGT (IU/L)	15.74 ± 0.9	83.63 ± 18.76 <sup>a</sup>	51.63 ± 18.37 <sup>a</sup>
TP (g/L)	74.05 ± 0.52	65.25 ± 1.41 <sup>a</sup>	53.08 ± 3.48 <sup>a,b</sup>
ALB (g/L)	48.26 ± 0.27	33.76 ± 0.86 <sup>a</sup>	22.83 ± 1.58 <sup>a,b</sup>
PALB (mg/L)	339.03 ± 3.95	169.64 ± 6.9 <sup>a</sup>	136.98 ± 23.47 <sup>a</sup>
TBA (μmol/L)	4.93 ± 0.29	57.77 ± 6.56 <sup>a</sup>	98.75 ± 17.67 <sup>a,b</sup>
CHE (KU/L)		5.01 ± 0.26	2.08 ± 0.3 <sup>b</sup>
Renal function			
CREA (μmol/L)	75.54 ± 0.79	69.9 ± 2.63	87.26 ± 16.58 <sup>a,b</sup>
BUN (mmol/L)	5.05 ± 0.13	4.66 ± 0.22	7.2 ± 1.56 <sup>a,b</sup>
UA (mmol/L)	309.58 ± 61.59	315.48 ± 126.70	278.21 ± 146.31
Blood lipids			
CHOL (mmol/L)	5.46 ± 0.11	4.4 ± 0.21 <sup>a</sup>	2.57 ± 0.31 <sup>a,b</sup>
TG (mmol/L)	1.6 ± 0.06	1.19 ± 0.09 <sup>a</sup>	1.01 ± 0.08 <sup>a</sup>
HDLC (mmol/L)	1.25 ± 0.23	1.04 ± 0.03 <sup>a</sup>	0.64 ± 0.07 <sup>a,b</sup>
LDLC (mmol/L)	3.44 ± 0.056	2.9 ± 0.11 <sup>a</sup>	1.93 ± 0.17 <sup>a,b</sup>
ApoA1 (g/L)		1.15 ± 0.03	0.72 ± 0.1
ApoB (g/L)		0.93 ± 0.03	0.71 ± 0.02
Blood glucose			
GLU (mmol/L)	5.51 ± 0.11	5.48 ± 0.15	6.75 ± 1.51 <sup>a</sup>
Coagulation function			
PT (Sec)		16.05 ± 0.4	22.75 ± 2.26 <sup>b</sup>
PTA (%)		72.46 ± 3.06	36.34 ± 6.57 <sup>b</sup>
PTR (%)		1.18 ± 0.02	1.35 ± 0.03 <sup>b</sup>
APTT (Sec)		42.05 ± 0.89	57.54 ± 5.31 <sup>b</sup>
TT (Sec)		22.19 ± 0.81	34.87 ± 3.32 <sup>b</sup>
FIB (g/L)		2.71 ± 0.07	1.63 ± 0.11 <sup>b</sup>
INR (%)		1.17 ± 0.02	1.63 ± 0.15 <sup>b</sup>
Blood tests			
RBC (10 <sup>12</sup> /L)	4.64 ± 0.05	3.95 ± 0.08 <sup>a</sup>	2.71 ± 0.13 <sup>a,b</sup>
WBC (10 <sup>9</sup> /L)	6.53 ± 0.17	4.54 ± 0.22 <sup>a</sup>	4.82 ± 0.85 <sup>a</sup>
HCT (%)	43.67 ± 0.45	38.03 ± 0.63 <sup>a</sup>	29.57 ± 1.59 <sup>a,b</sup>
HGB (g/L)	138.12 ± 2.3	115.58 ± 3.17	73.92 ± 6.97
MCH (pg)	28.16 ± 0.2	30.95 ± 0.31 <sup>a</sup>	32.5 ± 1.42 <sup>a</sup>
MCHC (g/L)	352.5 ± 0.93	339.57 ± 2.03 <sup>a</sup>	342.49 ± 7.4 <sup>a</sup>
MPV (fL)	8.17 ± 0.06	9.55 ± 0.14 <sup>a</sup>	8.98 ± 0.24 <sup>a</sup>
PLT (10 <sup>9</sup> /L)	267.35 ± 8.3	95.6 ± 6.97 <sup>a</sup>	72.07 ± 16.16 <sup>a</sup>
PCT (%)	0.14 ± 0.01	0.08 ± 0 <sup>a</sup>	0.06 ± 0 <sup>a,b</sup>
PDW (%)	15.35 ± 0.05	16.45 ± 0.12 <sup>a</sup>	16.85 ± 0.5 <sup>a</sup>

Note: Data are represented as Mean ± SEM. <sup>a</sup> *p* < .05 when compared to healthy controls; <sup>b</sup> *p* < .05, when cirrhosis patients with HE compared to patients without HE.

ALT, Alanine transaminase; AST, Aspartate transaminase; TBIL, Total bilirubin; DBIL, direct bilirubin; IBIL, indirect bilirubin; ALP, alkaline phosphatase; GGT, gamma-glutamyl transferase; TP, Total Protein; ALB, Albumin; PALB, prealbumin; TBA, Total bile acid; CHE, cholinesterase; CREA, creatinine; BUN, Blood urea nitrogen; UA, uric acid; CHOL, cholesterol; TG, Triglyceride; HDLC, High-Density Lipoprotein Cholesterol; LDLC, low-density lipoprotein cholesterol; ApoA1, Apolipoprotein A1; ApoB, Apolipoprotein B; GLU, Glucose; PT, Prothrombin Time; PTA, Prothrombin Time activity; PTR, Prothrombin Time Ratio; APTT, activated partial thromboplastin time; TT, thrombin time; Fib, Fibrinogen; INR, International Normalized Ratio; RBC, red blood cell; WBC, white blood cell; HCT, hematocrit; HGB, hemoglobin; MCH, mean corpuscular hemoglobin; MCHC, Mean corpuscular hemoglobin concentration; MPV, Mean platelet volume; PLT, platelet; PCT, plateletocrit; PDW, platelet distribution width.

### 3.2. STZ-HFD-induced NASH-HCC mice

The histology of livers harvested from STZ-HFD-induced NASH-HCC mice were examined at 4 time points using H&E staining (Fig. 2A). Consistent with the results in our previous publication [4], fatty liver

without inflammatory foci was observed at 6 weeks of age (2 weeks after STZ-HFD treatment), fatty liver with moderate neutrophils, lymphocytes and monocytes infiltration, and ballooning degeneration of hepatocytes was found at age of 8 weeks, and chronic fibrosis and HCC were found at ages of 12 and 20 weeks, respectively. ALT levels were significantly higher in NASH-HCC mice than the normal (Fig. 2F).

Brain samples were harvested at each time point for immunofluorescent and immunohistochemical staining for glial fibrillary acidic protein (GFAP) and NeuN (Fig. 2B, Fig. S3). GFAP is a principal component of astrocyte intermediate filaments and decreases of GFAP expression in the brain have been observed [31,32] in both acute and chronic liver damage. NeuN, a mature neuron marker that can be used to assess neuronal cell loss during HE [33–35], and has also been used to identify functional neurons in the CA1 [36], was found to be decreased with liver disease progression. Consistent with previous studies [31–33,35], the density of NeuN- and GFAP-positive cells in the brain of NASH-HCC mice reduced to about 50% of those in the normal control mice across all time points (Fig. 2C, D). We confirmed using western blot that the protein expression of NeuN and GFAP was significantly decreased in NASH-HCC mice compared to the normal control (Fig. S4). Immunofluorescent staining also showed significantly increased expression of ASBT in the brain of NASH-HCC mice (Fig. 2E).

Heatmap on individual BAs revealed markedly distinct patterns between groups in plasma, brain, liver and feces (Fig. 2G and Fig. S5). Notably, the ratio of conjugated BAs to unconjugated BAs significantly increased in NASH-HCC mice in plasma, brain, and liver, but decreased in feces, and the concentrations of hydrophobic BAs, including TCDCA, TCA and GCA, also increased in plasma, brain, and liver, but decreased at some early time points and increased at the end in feces (Fig. 2G and Fig. S5). Compared with the normal mice, NASH-HCC mice had significantly higher levels of total BAs in plasma at all four time points, in liver and brain, but in feces, only at the later time points (Fig. 2H–2K).

Gene expression analysis showed that there were significantly up-regulated expression of ASBT in the ileum and brain, and significantly upregulated OST-α in the ileum but downregulated OST-α and OST-β in the brain (Fig. 2L–M and Fig. S6). Gene expression of NTCP significantly decreased in the liver (Fig. S6). Importantly, markedly increased intestinal pH along with the significantly increased serum ammonia levels were observed in the STZ-HFD mice compared to normal controls (Fig. 2N–O).

To test our hypothesis that ASBT plays a critical role in BA reabsorption and HE development, we treated the NASH-HCC mice with ASBT inhibitor SC-435 from week 4 to week 20. In agreement with previous studies [37,38], ileal BA absorption was inhibited by SC-435 treatment. Compared to the STZ-HFD-fed mice, SC-435 treated mice had less liver damages (Fig. 3A and B) and less reduction in astrogliosis in brain as evidenced by significantly increased expression of GFAP (Fig. 3C, D). Immunofluorescent and immunohistochemical staining also showed significantly decreased expression of GFAP and NeuN in STZ-HFD-fed mice but they were normalized by SC-435 treatment (Figs. 3C–3F, S7). Western blot also confirmed that the protein expression of NeuN and GFAP was significantly decreased in NASH-HCC mice compared to the normal control but normalized after SC-435 intervention (Fig. S8). Elevated ALT levels in NASH-HCC mice were also partially normalized by SC-435 (Fig. 3G). Total BA levels in serum, liver, and brain were significantly increased in STZ-HFD mice but were attenuated after SC-435 treatment (Fig. 3H–3J). Serum and brain ammonia levels decreased by 45% and 26%, respectively, after the SC-435 intervention, although the SC-435-induced changes were not statistically significant (*p* = .26) (Fig. 3K, L). ASBT protein expression in brain was upregulated in NASH-HCC mice, but was normalized by SC-435 treatment (Fig. 3M). Brain injuries are associated with anxiety disorders in both humans [39] and rodents [40]. As expected, NASH-HCC mice spent more time in the closed arms of the elevated plus maze than normal mice, indicating higher anxiety levels in these mice, and SC-435 treatment decreased

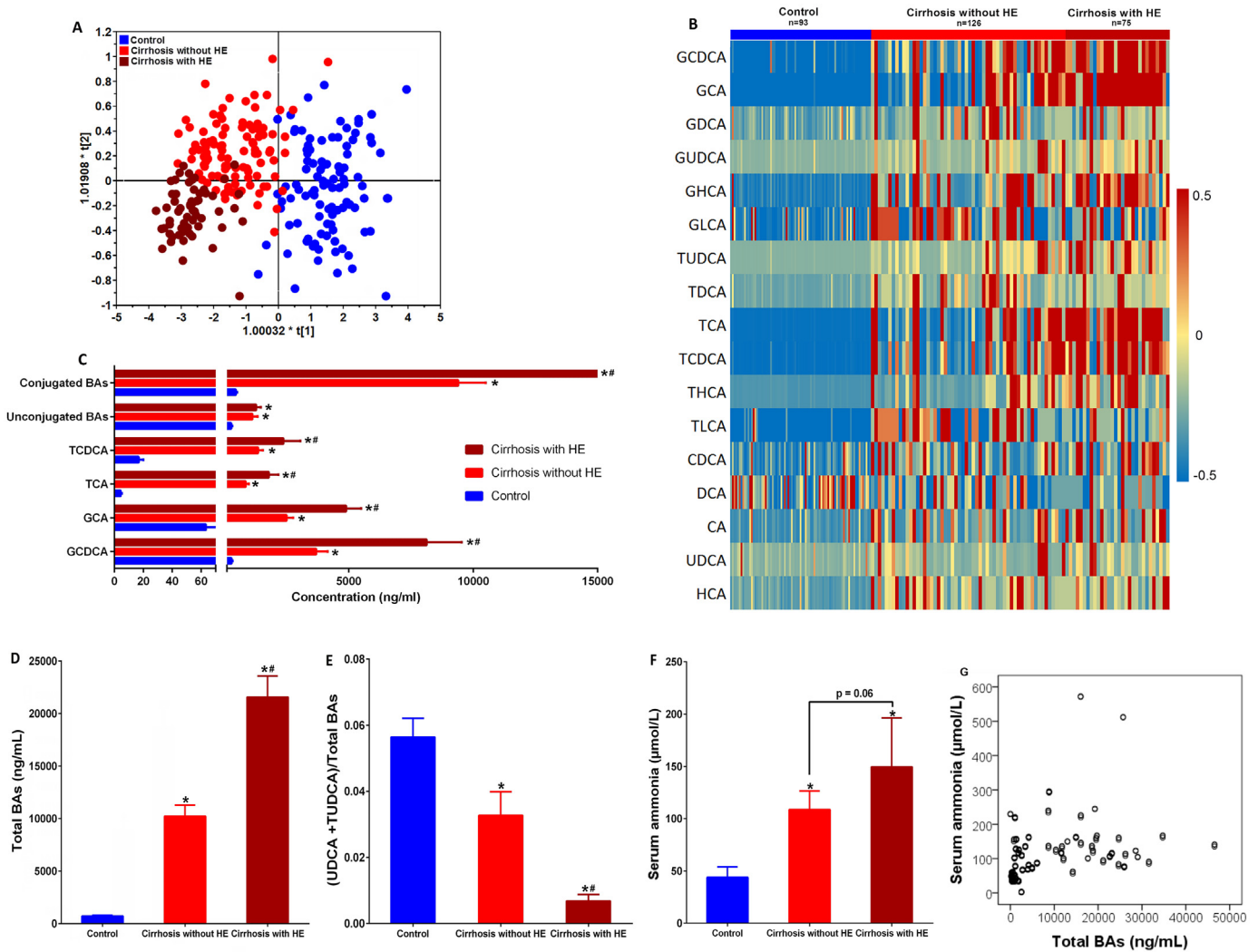


**Fig. 1.** Serum BAs and ammonia increased significantly in liver cirrhosis patients with ( $n = 75$ ) or without ( $n = 126$ ) HE compared with healthy controls ( $n = 93$ ). (A) OPLS-DA results for the three groups, control, cirrhosis patients with and without HE using all the identified BAs. (B) Heatmap of the individual BA concentrations (log-transformed). Shades of red and blue represented high or low BA concentration (see colour scale). (C) Conjugated BAs, unconjugated BAs, TCA, TCDC, GCA and GCDCA levels in sera. (D) Total BA levels in sera. (E) The proportion of UDCA and TUDCA in total BAs in sera. (F) Serum ammonia levels. (G) Scatter plot of serum concentrations of the total BAs against serum concentrations of ammonia. Data are represented as Mean  $\pm$  SEM. \* Values significantly different from controls,  $p < .01$ . # Values significantly different between cirrhosis patients with or without HE,  $p < .01$ .

the time in the closed arms by 37%, but this change was not statistically significant ( $p = .18$ ) (Fig. 3N).

### 3.3. AOM-induced acute liver failure mice

H&E staining of liver tissue showed that AOM treatment resulted in profound centrilobular necrosis along with vacuolar degeneration of hepatocytes, SC-435 treatment ameliorate and budesonide treatment aggravated the observed liver damages (Fig. 4A). All 3 groups of treated mice had significantly elevated ALT levels compared with normal controls, but in reference to AOM mice, ALT level increased by 33% in AOM/Budesonide mice, and decreased by 20% in AOM/SC-435 mice (Fig. 4B). H&E staining of brain tissue showed that compared with the normal controls, AOM-treated mice had ballooning and twinning astrocytes (Fig. 4C, S9, markers of central nervous system edema) and decreased protein expression of GFAP (Fig. 4D, E) and NeuN (Fig. 4F, G) from immunofluorescent and immunohistochemical analysis. In reference to AOM mice, budesonide further decreased and SC-435 increased protein expression of GFAP and NeuN. AOM- and AOM/Budesonide-treated mice showed higher levels of anxiety than normal, as indicated by less time spent in the open arms of the elevated plus

maze, and the SC-435 treatment alleviated anxiety in the AOM-treated mice (Fig. 4H). The AOM mice had lower survival rate than normal control mice, while budesonide further decreased and SC-435 improved the survival rate of AOM mice (Fig. 4I).

AOM treatment significantly elevated total BAs in serum, liver, and brain, and these changes in concentrations seemed to be further aggravated by budesonide, and partially prevented by SC-435 (Fig. 4J–4L). Examination of ileum content revealed that the lowest level of total BAs and the highest level of pH were both found in the AOM/Budesonide mice, which correlated with the highest level of serum ammonia for this group (Fig. 4M–4O). Fig. S10 shows that the amounts of cytotoxic BAs, such as TCA, TCDC, TDCA and DCA, significantly increased in serum, liver and brain after AOM and AOM/budesonide treatments, and these changes were partially prevented by SC-435 (Fig. 4J–4L). Conversely, TUDCA, as a neuroprotective BA, decreased in liver and brain of AOM and AOM/budesonide mice. All these aforementioned individual BAs showed lower levels in the intestinal content of AOM and AOM/budesonide mice than in normal control mice, while SC-435 treatment seemed to have partially improved this situation.

AOM treatment also upregulated gene expression of ASBT in the ileum (Fig. 4Q) and brain (Fig. 4R), which was exacerbated by

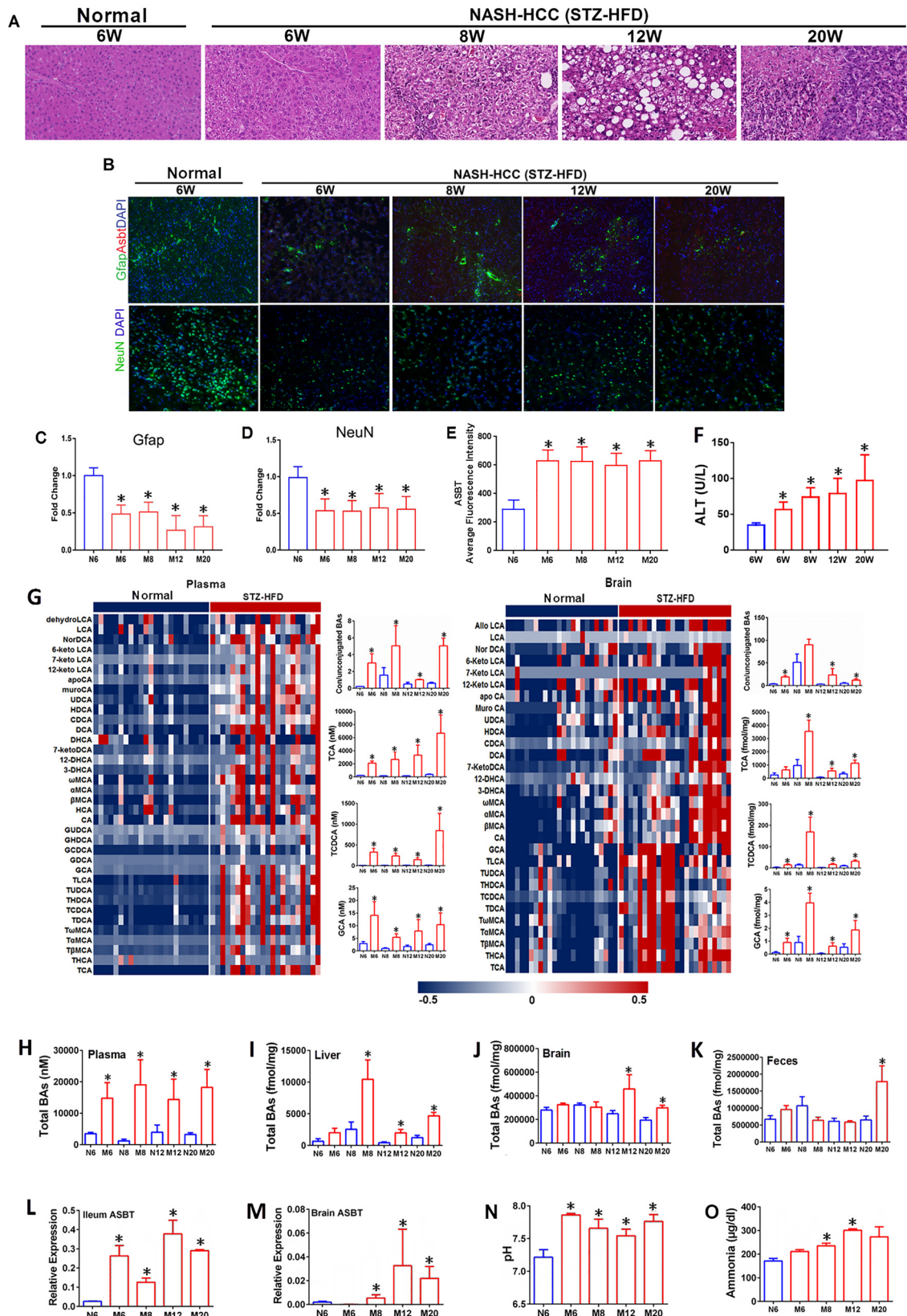


**Fig. 2.** The characterization of ASBT, NeuN, GFAP, BAs and ALT in the STZ-HFD-induced NASH-HCC mice. (A) H&E stained liver sections from normal ( $n = 8$ ) and NASH-HCC mice ( $n = 8$ ) at weeks 6, 8, 12 and 20. Original magnifications 200 $\times$ . (B) Fluorescence immunostaining of ASBT (red) costained with neuronal marker NeuN or GFAP (green) in the cortices of normal and NASH-HCC mice at ages of 6, 8, 12, and 20 weeks. (C,D) The densities of GFAP- and NeuN-positive cells dramatically reduced in model mice ( $n = 6$ ;  $p < .05$ ). (E) Immunofluorescent staining show significantly increased expression of ASBT in the brain of NASH-HCC mice. (F) ALT levels in NASH-HCC mice. (G) Heatmap of individual BA concentrations (log-transformed) in plasma and brain. Shades of red and blue represented high or low BA concentration (see colour scale). (H–K) Total BAs level in plasma, brain, liver and feces were increased. (L–O) Ileum and brain ASBT, intestinal pH and serum ammonium were significantly increased in model mice. \*,  $p < .05$ , vs. normal ( $n = 6$ ).

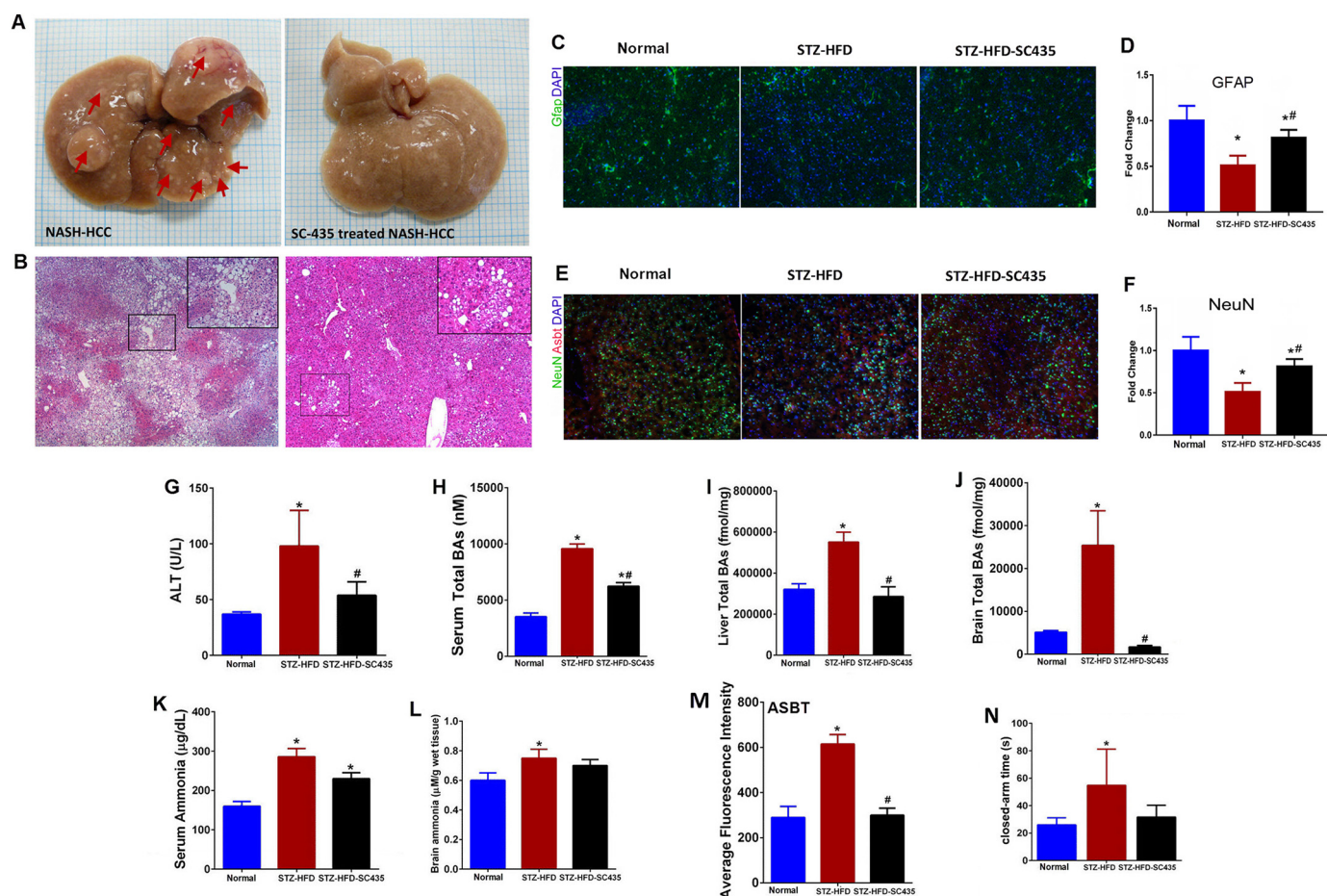


**Fig. 3.** SC-435 treatment on STZ-HFD-induced HCC mice. (A) SC-435 treatment inhibited the development of HCC in the livers of STZ-HFD mice ( $n = 6$ ). (B) H&E stained liver sections from STZ-HFD mice with or without SC-435 treatment at age 20 weeks. (C, E) Fluorescence immunostaining of ASBT (red) costained with neuronal marker NeuN or GFAP (green) in the cortices of normal and STZ-HFD mice with or without SC-435 treatment at age 20 weeks. (D, F) The densities of GFAP- and NeuN-positive cells dramatically reduced in model mice ( $n = 6$ ). (G) Levels of ALT elevated in STZ-HFD mice, with or without SC-435 treatment, compared with normal. (H–J) Concentrations of total BAs in serum, liver and brain increased in STZ-HFD mice, but this change was ameliorated by SC-435 treatment. (K, L) Serum and brain ammonia levels increased in STZ-HFD mice with or without SC-435 treatment. (M) Brain ASBT levels. (N) STZ-HFD mice without SC-435 treatment spent more time in the closed-arms in elevated plus maze test, implicating higher level of anxiety. \*,  $p < .05$ , compared to normal group ( $n = 6$ ); #,  $p < .05$ , compared to STZ-HFD group.

budesonide and inhibited by SC-435. The gene expression of OST- $\beta$  in ileum was also upregulated by AOM and AOM/budesonide, and normalized by SC-435 (Fig. 4S). Upregulated gene expression of farnesoid X receptor (FXR) was observed in the brain (Fig. 4T) while downregulated FXR was detected in the liver (Fig. 4P) in AOM/budesonide mice.

IHC staining showed significantly decreased protein expression of the hepatic BA transporter, Ntcp in AOM- and AOM/Budesonide-treated mice compared with normal, and the expression levels were normalized in AOM/SC-435-treated mice (Fig. S11).

### 3.4. Increased proportion of intestinal conjugated BAs in AOM mice enhanced ASBT expression via decreased FXR activation

We found that the proportions of conjugated BAs such as TCA, TCDCa, TDCA were much higher (TCA/CA = 26.25; TCDCa/CDCA = 4.4; TDCA/DCA = 5.87) in intestinal contents of AOM mice than in normal controls (Fig. 5A), although their absolute concentration in intestinal contents were lower (Fig. S10). Based on the findings of significantly increased ileal ASBT expression in AOM mice, we treated cecal epithelial CLL-251 cells with 50  $\mu$ M of CA, CDCA, LCA, DCA, UDCA and their taurine and glycine conjugates for 48 h. The conjugated BAs showed higher activation levels of ASBT protein expression than the unconjugated BAs, except for UDCA and its conjugates (Fig. 5B).

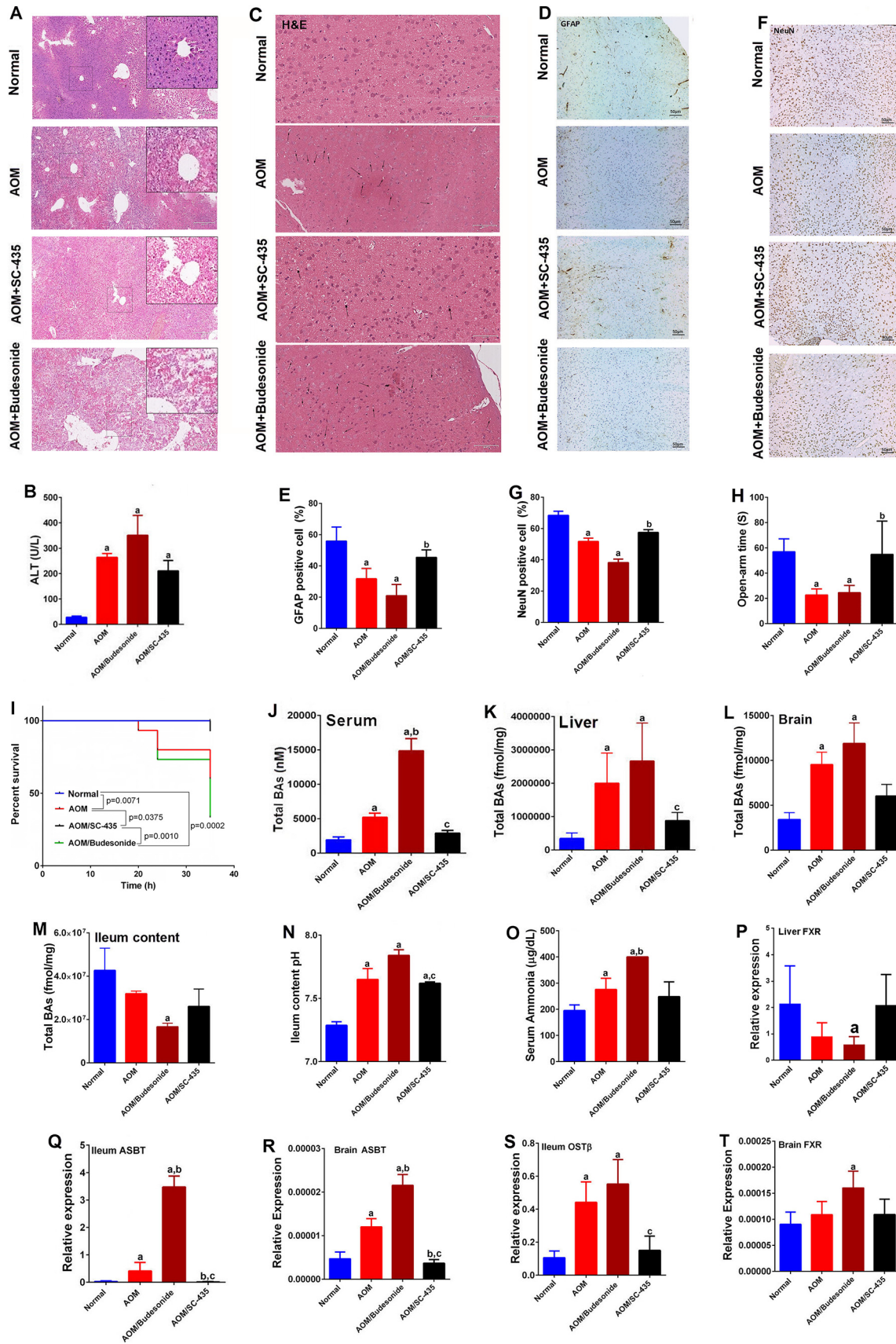
We further treated CLL-251 cells with combined unconjugated BAs and combined conjugated BAs (CA + CDCA, TCA + GCA + TCDCa

+GDCA, DCA + LCA, and TDCA+GDCA+TLCA+GLCA) in a 3D culture system for up to 7 days. Immunofluorescent staining showed that conjugated BAs upregulated protein expression of ASBT but downregulated that of FXR while unconjugated BAs suppressed ASBT expression but upregulated FXR (Fig. 5C).

We used the GW4064 (FXR agonist, 100 nM) to reactivate FXR in TDCA+GDCA+TLCA+GLCA treated CLL-251 cells, and (Z)-Guggulsterone (FXR antagonist, 20  $\mu$ M) to suppress FXR in CA and CDCA treated CLL-251 cells. The data shown in Fig. 5D and E indicate that upregulated protein expression of ASBT by TDCA+GDCA+TLCA+GLCA treatment was attenuated after GW4064 treatment while suppressed ASBT expression by CA and CDCA treatments was significantly recovered with (Z)-Guggulsterone treatment. These results indicated that conjugated BAs upregulated intestinal ASBT activity via the inhibition of intestinal FXR. The increased ASBT mediated BA reabsorption through suppression of intestinal FXR signaling by conjugated BAs is further supported by the observation that AOM mice had higher ASBT expression and lower FXR expression in their intestine tissues, in reference to normal controls (Fig. 5F).

### 3.5. Budesonide treatment on normal mice

To confirm that activation of ileal BA absorption could increase BAs and ammonia in the blood and brain, we fed normal mice with budesonide for one week. H&E staining showed that budesonide



induced hepatocyte swelling/ballooning (Fig. 6A), also increased ALT and AST serum levels (Fig. 6B). Meanwhile, the protein expression of GFAP in brain tissue decreased in budesonide treated normal mice

(Fig. 6C), and these mice also showed higher anxiety level than normal controls, as evidenced by the result of the elevated plus maze test (Fig. 6D). Budesonide treatment increased the total BAs levels in

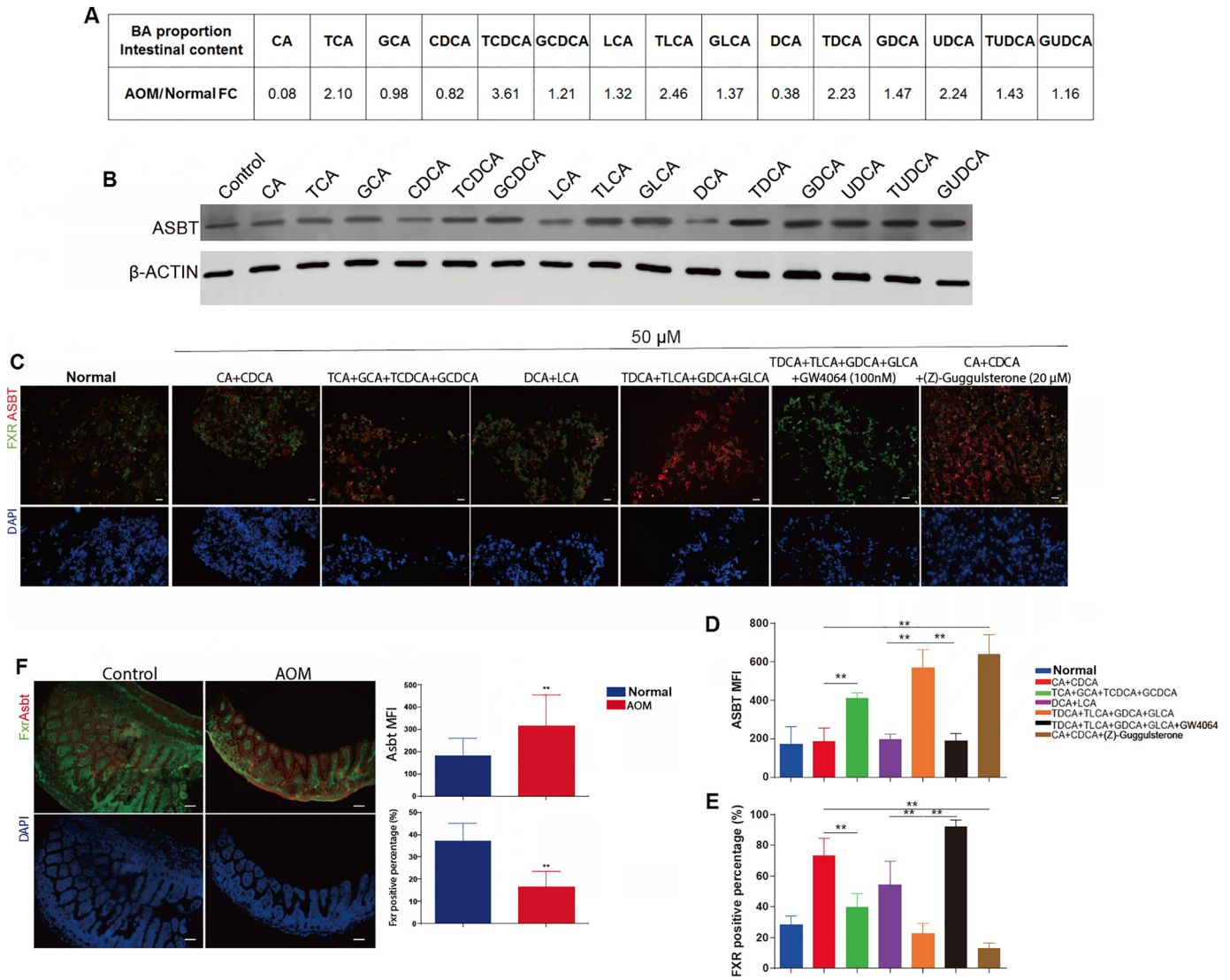


**Fig. 5.** Regulatory effects of unconjugated and conjugated BAs on ASBT and FXR protein expression. (A) Proportion of different BAs in intestinal content in AOM mice and normal controls. FC was calculated as the ratio AOM/normal of the average proportion of BAs. (B) Western-blot analysis of the expression of ASBT in human cecum epithelial cell line CLL-251 treated with 5 groups of BAs (5 unconjugated BAs and their taurine and glycine conjugates, 50  $\mu$ M, 48 h). Beta-actin was used as loading control. (C, D, E) The expression of ASBT and FXR in the CLL-251 3D micro-tissues with different indicated treatments detected by immunofluorescent staining. (F) Immunofluorescent staining of mouse intestine tissues in normal and AOM mice for the expression of ASBT and FXR. The mean of fluorescence Intensity (MFI) of ASBT and FXR nuclear positive cells percentage were calculated by Image J.

serum, liver, and brain, and decreased them in intestinal content (Fig. 6E). Budesonide also increased ammonia levels in serum, cecum and brain (Fig. 6F), and upregulated ASBT gene expression in the ileum (Fig. 6G).

Fig. S12 shows that the amounts of cytotoxic BAs (TCA, TCDCa, TDCA and DCA) significantly increased in serum, liver and brain after budesonide treatment, but the concentration of neuroprotective TUDCA decreased in the brain of the budesonide treated mice. Notably all the individual BAs mentioned above had significantly lower

concentrations in the ileum of the budesonide treated mice than in the normal mice.

#### 4. Discussion

Current treatment options for HE are limited and there is an urgent need to identify better targets for therapeutic intervention. This study demonstrated that 1) conjugated BAs significantly elevated in sera of liver cirrhosis patients, and further elevated in those with HE; 2) ASBT

**Fig. 4.** Liver and brain damage in AOM-induced acute liver failure model mice. (A) H&E staining of normal mouse liver, liver section from a preterminal stage IV HE mouse 35 h after exposure to AOM, liver section from a mouse 35 h after exposure to AOM and previous administration of budesonide or SC-435 for 5 days (Magnif. 200 $\times$ ). (B) ALT levels in C57BL/6 J mice with HE due to AOM-induced liver failure. (C) H&E staining of a brain section of a healthy control mouse, brain section of a mouse exposed to AOM for 35 h (stage IV HE), AOM + SC-435 mice and AOM-budesonide mice showing astrocyte ballooning and twinning (arrow). Bar scale: 73  $\mu$ m. (D) Immunohistochemistry for GFAP on a brain section from a normal mouse, in stage IV HE AOM mice, AOM + SC-435 mice and AOM-budesonide mice. (E) GFAP positive cell percentage in three groups. (F) Immunohistochemistry for NeuN on a brain section from a normal mouse, in stage IV HE AOM mice, AOM + SC-435 mice and AOM-budesonide mice. (G) NeuN positive cell percentage in three groups. (H) Time (s) spent in the open arms of the maze at different groups. (I) Survival rates of mice treated with vehicle, AOM, AOM + SC-435, and AOM + Budesonide. (J, K, L, M) Total BAs in serum, liver and brain were significantly increased while total BAs in ileum content were significantly decreased in AOM-induced model mice and were further increased by budesonide treatment but were normalized after the SC-435 intervention. (N) Ileum content pH of the 4 study groups. (O) Serum ammonia levels of the 4 study groups. (P) Liver FXR levels. (Q, R, S, T) Ileum and brain BA transporters were significantly increased in AOM-induced model mice and were further increased by budesonide treatment but were normalized after the SC-435 intervention. <sup>a</sup>,  $p < .05$ , compared to normal group; <sup>b</sup>,  $p < .05$ , compared to AOM group; <sup>c</sup>,  $p < .05$ , compared to AOM/Budesonide group.

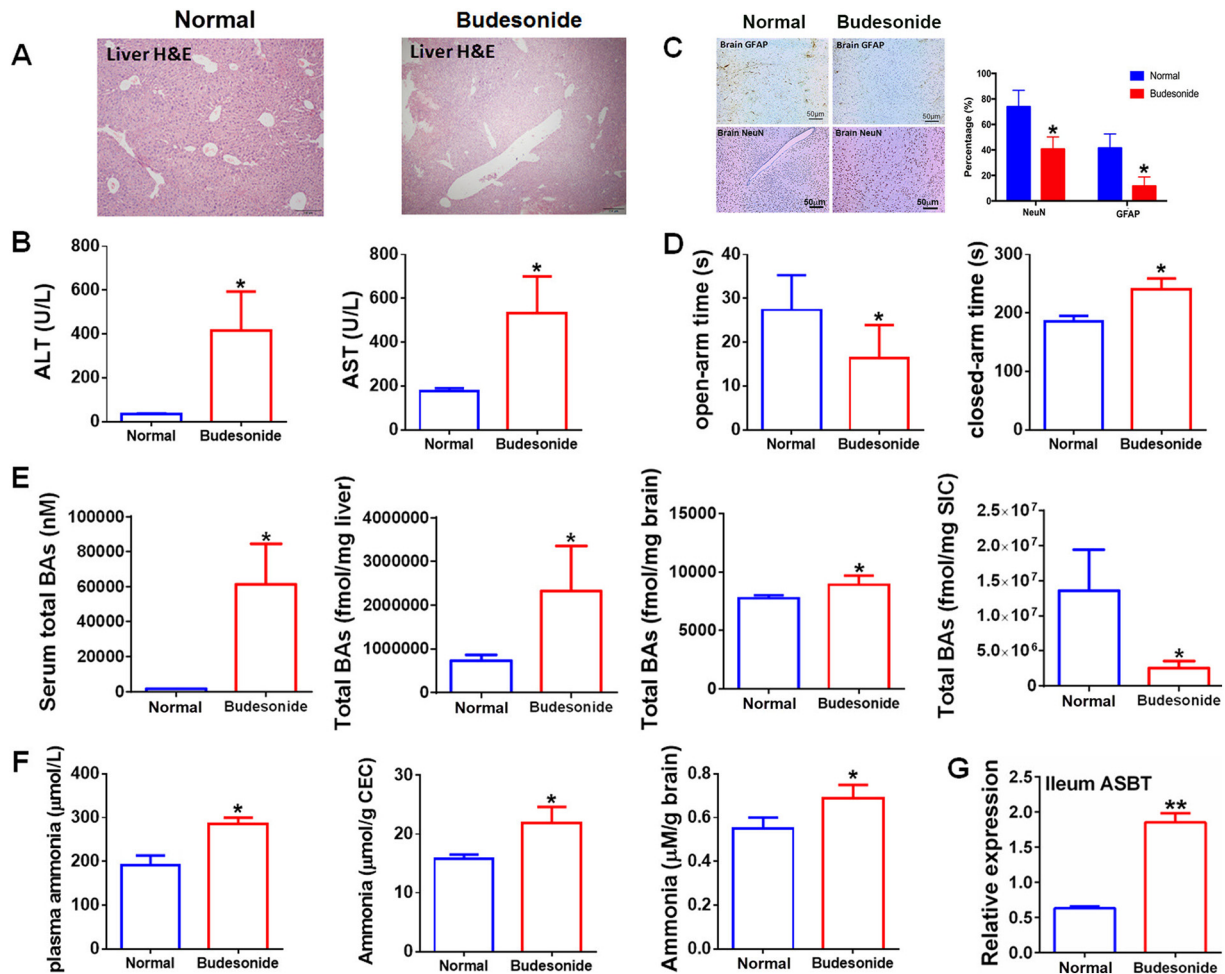


**Fig. 6.** Budesonide treatment on C57BL/6J normal mice. (A) H&E stained liver sections from normal and budesonide treated mice. (B) Serum levels of ALT and AST in normal and budesonide treated mice. (C) Immunohistochemical staining for GFAP on a brain section from a normal mouse, and a budesonide treated mouse. (D) Times (s) spent in open-arm and closed-arm tray. (E) Total BAs in serum, intestinal content (SIC), liver, and brain. (F). Serum, cecal (CEC) and brain ammonia levels. (G) Ileum ASBT gene expression. Data are presented as mean  $\pm$  SEM. \*,  $p < .05$ , compared to normal group.

gene expression in the ileum and BA concentrations in blood, liver, and brain were significantly increased in a chronic liver disease mouse model (STZ-HFD) as well as an AOM-induced ALF mouse model; 3) ASBT mediated BA reabsorption increased pH in the ileum, leading to abnormally high levels of cytotoxic BAs and neurotoxic ammonia in blood and brain, contributing to the neurological impairment; and 4) blockage of intestinal BA reabsorption via inhibiting ileal ASBT significantly alleviated liver and brain damage as evidenced by lowered BA concentrations, and increased GFAP- and NeuN-positive cells in brain (Fig. 7). Taken together, our data showed that dysregulated BA signaling due to ALF or chronic liver disease may contribute to HE because inhibition of enteric BA reabsorption reduces the circulating BAs and thus, thus protected against the development of HE.

Blood ammonia levels are used for diagnosis and treatment evaluation of HE [41]. Ammonia is mainly produced in the gut [42], where bacterial deamination of amino acids and bacterial urease metabolism of liver derived urea takes place. Under normal conditions, ammonia is partially reabsorbed by the colon and enters the blood circulation [43]. The homeostasis of ammonia is profoundly altered in liver failure resulting in hyperammonemia due to excessive ammonia released from the intestine and to deficient ammonium clearance by the diseased liver with impaired urea cycle. Abnormally high circulating ammonia leads to excessive cerebral ammonia uptake which in turn, leads to cerebral edema and the development of HE [44]. Our study revealed that a simple but key factor that controls the intestinal reabsorption of ammonia is the intestinal luminal pH. Under acidic ( $pH < 6$ ) or

physiological conditions ammonia exists mainly as the ionized form,  $NH_4^+$ , and is readily excreted in the feces. However, under basic conditions, intestinal ammonia will be converted to  $NH_3$ , which can diffuse freely through the cytoplasm membrane, and its reabsorption from colon into blood circulation increases with increased pH [45,46]. The intraluminal pH varies from highly acidic in the stomach to mildly acidic conditions in the proximal colon and to more neutral pH distally. BAs play a key role in regulating intestinal pH due to their strong acidity ( $pK_a \sim 1-7$ ) [47], sustained concentration levels and distribution throughout the intestine. In advanced liver diseases such as cirrhosis, the enterohepatic circulation of BAs is impaired with downregulated hepatic production and upregulated intestinal reabsorption of BAs. Our study showed both NASH-HCC and HE model mice had lower BA levels in the intestines than normal mice, along with higher levels of intestinal pH and blood ammonia.

We found that ASBT expression was significantly upregulated in the brain in AOM-treated mice, which is consistent with a prior study reporting increased expression of ASBT in the cortices of these mice [6]. ASBT has been reported to have a higher affinity for the taurine and glycine conjugates over the unconjugated forms [48], which supports our findings that conjugated BAs increased significantly in HE patients and mice with markedly increased ASBT expression. UDCA and TUDCA are neuroprotective hydrophilic BAs [49,50], and we showed that the AOM-induced HE model mice had significantly decreased TUDCA levels in the brain and HE patients had significantly decreased proportion of UDCA and TUDCA in serum BAs.

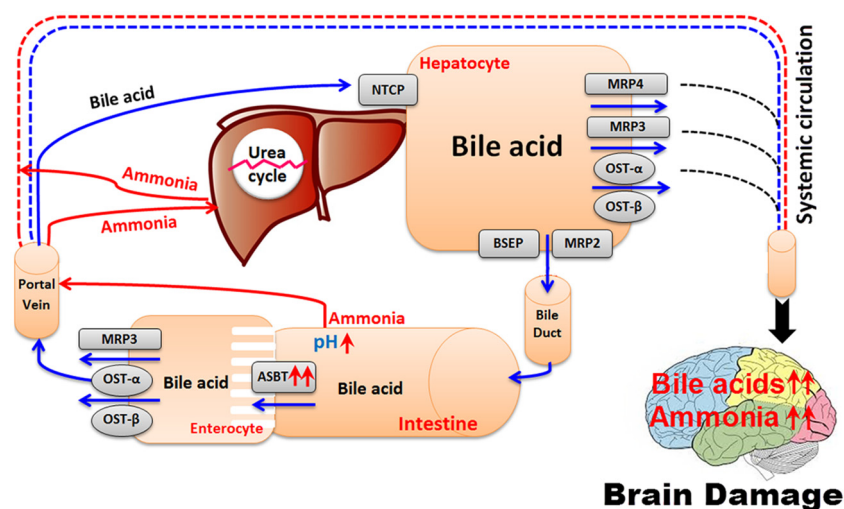


**Fig. 7.** A proposed model for the hypothesis that significant increases in ASBT mediated BA reabsorption and subsequent increased pH in the ileum and colon will lead to abnormally high levels of cytotoxic BAs and neurotoxic ammonia in blood and brain that further induce brain damage. Arrows in red: ammonia metabolism. Arrows in blue: bile acid metabolism.

It is generally considered that liver failure may be associated with altered neurological function, but not necessarily with neuronal loss. Thus, measurement of neuronal loss may not be sufficient to represent the neurological symptoms characteristic of HE. However, neuronal loss including neuronal cell damage and death has been well documented in liver failure patients, in the form of several distinct clinical entities namely acquired (non-Wilsonian) hepatocerebral degeneration, cirrhosis-related Parkinsonism, post-shunt myelopathy, and cerebellar degeneration [51,52]. Cerebellar degeneration, with loss of Purkinje neurons was also reported in 20 out of 36 patients who died with liver cirrhosis and HE [33]. There was neuronal loss in the deeper cerebral cortical layers and the basal ganglia as well as microcavitation in the dentate nucleus in HE patients [34]. Results on 48 patients with cirrhosis without overt hepatic encephalopathy and 51 age and sex-matched healthy subjects indicated that loss of brain tissue density is common in cirrhosis, progresses during the course of the disease, is greater in patients with history of hepatic encephalopathy, and persists after liver transplantation [35]. A recent study also showed that patients with chronic liver disease show infiltration of Th17 and Tfh lymphocytes in the meninges in cerebellum, microglia and astroglia activation and the loss of Purkinje and granular neurons [53]. Neuronal loss, especially in cerebellum, is therefore more frequent than previously assumed in liver disease.

Although the STZ-HFD induced NASH-HCC mouse model is not a well-established HE model, we observed brain damages in these mice such as evidenced by significantly decreased GFAP and NeuN protein expression in brain tissues compared with normal control mice. We also observed that STZ-HFD treatment upregulated ASBT expression in ileum and brain, significantly elevated ileal pH and blood ammonia concentration, and markedly increased cytotoxic BAs in the brain. These characteristics were similar to the results found in AOM mice, suggesting STZ-HFD treatment also induced neurological decline in C57BL/6J mice. It is noteworthy that the mitigation of liver disease was most likely the reason for the attenuation of ALT and serum ammonia levels and that examination of the reason for the greater effectiveness of SC-435 on the AOM model mice vs. STZ-HFD mice warrants further investigation.

Treatment with SC-435 decreased blood and brain ammonia and the anxiety levels in model mice. Currently, it is unclear that all the observed neurological improvements were due to improved liver function, improved brain function, or both, which warrants further investigation. ASBT gene expression is also regulated by the glucocorticoid receptor [22]. Glucocorticoids are primary stress hormones, and their circulatory levels have been shown to increase in response to both physiological [54] and psychological [55] stress factors. Therefore, such stresses may accelerate intestinal BA absorption via glucocorticoid receptor-

mediated ASBT upregulation in the ileum. Budesonide, a corticosteroid exhibits potent glucocorticoid receptor activity [56], and this may explain some of its ability to upregulate ASBT expression and increase BA reabsorption by the intestine.

Recent studies have revealed that multiple neurological disorders, including Parkinson's disease and Alzheimer's disease, are closely associated with the abnormal BA metabolism and biodistribution [57,58]. Targeting ASBT may, therefore, become a novel therapeutic approach for chronic neurological conditions that often exhibit an impaired BA regulation.

In summary, our study showed elevated concentrations of conjugated BAs and ammonia in the sera of liver cirrhosis patients with HE compared with those without HE. Animal studies further demonstrated that ASBT activation enhanced intestinal reabsorption of BAs and increased concentrations of BAs and ammonia in both blood and brain, resulting in brain tissue damage. Conversely, blocking BA reabsorption from the intestine via inhibiting ASBT decreased concentrations of BAs and ammonia in blood and brain in mice with liver damage and thus, ameliorated the neurological decline in these mice.

#### Acknowledgements

We wish to thank the research coordinators of the participating hospitals for their assistance in collecting clinical data and samples.

#### Financial statement

This study was financially supported by the National Key R&D Program of China (2017YFC0906800), the National Institutes of Health/National Cancer Institute Grant 1U01CA188387-01A1, the Key Program of National Natural Science Foundation of China (8153000502), the National Natural Science Foundation of China (81573873, 81774196, 81772530), China Postdoctoral Science Foundation funded project, China (2016T90381, 2015M581652), and E-institutes of Shanghai Municipal Education Commission, China (E03008).

#### Author contributions

W.J. was principal investigator of this study and designed the study. P. L. organized the patient recruitment and AOM and budesonide mouse experiment, and provided biospecimens for this study. G.X.X. conducted key experiments of the study and performed metabolomic profiling of bile acids and data analysis. X.N.W. conducted the mouse experiments and collected the data. R.Q.J. conducted the cell experiments and analyzed

the data. A.H.Z., J.Y.Y., X.J.Z., F.J.H., X.Z.L., and C.Y. helped to perform the experiments and collected the data. G.X.X. wrote the manuscript. G.X.X., J.P., C.R., H.Y., W.P.J., B.C.S. and W.J. critically revised the manuscript.

## Declaration of interests

The authors declare that they have no competing interests.

## Appendix A. Supplementary data

Supplementary data to this article can be found online at <https://doi.org/10.1016/j.ebiom.2018.10.030>.

## References

- Munoz SJ. Hepatic encephalopathy. *Med Clin North Am* 2008;92(4):795–812 [viii].
- Riordan SM, Williams R. Treatment of hepatic encephalopathy. *N Engl J Med* 1997; 337(7):473–9.
- Wang X, Xie G, Zhao A, et al. Serum Bile Acids are Associated with Pathological Progression of Hepatitis B-induced Cirrhosis. *J Proteome Res* 2016;15(4):1126–34.
- Xie G, Wang X, Huang F, et al. Dysregulated hepatic bile acids collaboratively promote liver carcinogenesis. *Int J Cancer* 2016;139(8):1764–75.
- Yin PY, Wan DF, Zhao CX, et al. A metabonomic study of hepatitis B-induced liver cirrhosis and hepatocellular carcinoma by using RP-LC and HILIC coupled with mass spectrometry. *Mol Biosyst* 2009;5(8):868–76.
- McMillin M, Frampton G, Quinn M, et al. Bile Acid Signaling is involved in the Neurological Decline in a Murine Model of Acute Liver failure. *Am J Pathol* 2016;186(2): 312–23.
- Bron B, Waldram R, Silk DB, Williams R. Serum, cerebrospinal fluid, and brain levels of bile acids in patients with fulminant hepatic failure. *Gut* 1977;18(9):692–6.
- Jia W, Xie G, Jia WP. Bile acid-microbiota crosstalk in gastrointestinal inflammation and carcinogenesis. *Nat Rev Gastroenterol Hepatol* 2018;15(2):111–28.
- Huff MW, Telford DE, Edwards JL, et al. Inhibition of the apical sodium-dependent bile acid transporter reduces LDL cholesterol and apoB by enhanced plasma clearance of LDL apoB. *Arterioscler Thromb Vasc Biol* 2002;22(11):1884–91.
- Craddock AL, Love MW, Daniel RW, et al. Expression and transport properties of the human ileal and renal sodium-dependent bile acid transporter. *Am J Physiol* 1998; 274(1 Pt 1):G157–69.
- Hruz P, Zimmermann C, Gutmann H, et al. Adaptive regulation of the ileal apical sodium dependent bile acid transporter (ASBT) in patients with obstructive cholestasis. *Gut* 2006;55(3):395–402.
- Trauner M, Boyer JL. Bile salt transporters: molecular characterization, function, and regulation. *Physiol Rev* 2003;83(2):633–71.
- Zheng X, Chen T, Zhao A, et al. The Brain Metabolome of Male Rats across the Lifespan. *Sci Rep* 2016;6:24125.
- Swann JR, Want EJ, Geier FM, et al. Systemic gut microbial modulation of bile acid metabolism in host tissue compartments. *Proc Natl Acad Sci U S A* 2011;114:4523–30.
- Ornft NW, Munk OL, Frisch K, Ott P, Keiding S, Sorensen M. Hepatobiliary transport kinetics of the conjugated bile acid tracer (11)C-CSar quantified in healthy humans and patients by positron emission tomography. *J Hepatol* 2017;67(2):321–7.
- Weiss N, Barbier Saint Hilaire P, Colsch B, et al. Cerebrospinal fluid metabolomics highlights dysregulation of energy metabolism in overt hepatic encephalopathy. *J Hepatol* 2016;65(6):1120–30.
- Huang F, Wang T, Lan Y, et al. Deletion of mouse FXR gene disturbs multiple neurotransmitter systems and alters neurobehavior. *Frontiers in Behavioral Neuroscience* 2015;9:70.
- Belanger M, Cote J, Butterworth RF. Neurobiological characterization of an azoxymethane mouse model of acute liver failure. *Neurochem Int* 2006;48(6–7): 434–40.
- Matkowskyj KA, Marrero JA, Carroll RE, Danilkovich AV, Green RM, Benya RV. Azoxymethane-induced fulminant hepatic failure in C57BL/6J mice: characterization of a new animal model. *Am J Physiol* 1999;277(2 Pt 1):G455–62.
- Fujii M, Shibazaki Y, Wakamatsu K, et al. A murine model for non-alcoholic steatohepatitis showing evidence of association between diabetes and hepatocellular carcinoma. *Med Mol Morphol* 2013;46(3):141–52.
- West KL, Ramjiganesh T, Roy S, Keller BT, Fernandez ML. 1-[4-[4(4R,5R)-3,3-Dibutyl-7-(dimethylamino)-2,3,4,5-tetrahydro-4-hydroxy-1,1-dioxido-1-benzothiepin-5-yl]phenoxy]butyl]-4-aza-1-azoniabicyclo[2.2.2]octane methanesulfonate (SC-435), an ileal apical sodium-coupled bile acid transporter inhibitor alters hepatic cholesterol metabolism and lowers plasma low-density lipoprotein-cholesterol concentrations in Guinea pigs. *J Pharmacol Exp Ther* 2002;303(1):293–9.
- Jung D, Fantin AC, Scheurer U, Fried M, Kullak-Ublick GA. Human ileal bile acid transporter gene ASBT (SLC10A2) is transactivated by the glucocorticoid receptor. *Gut* 2004;53(1):78–84.
- Bajor A, Kilander A, Galman C, Rudling M, Ung KA. Budesonide treatment is associated with increased bile acid absorption in collagenous colitis. *Aliment Pharmacol Ther* 2006;24(11–12):1643–9.
- Matkowskyj KA, Marrero JA, Carroll RE, Daniilkovich AV, Green RM, Benya RV. Azoxymethane-induced fulminant hepatic failure in C57BL/6J mice: characterization of a new animal model. *Am J Physiol* 1999;277(2 Pt 1):G455–62.
- Webster SJ, Bachstetter AD, Van Eldik LJ. Comprehensive behavioral characterization of an APP/PS-1 double knock-in mouse model of Alzheimer's disease. *Alzheimer's Research & Therapy* 2013;5(3):28.
- Xie G, Zhong W, Li H, et al. Alteration of bile acid metabolism in the rat induced by chronic ethanol consumption. *FASEB Journal* 2013;27(9):3583–93.
- Tang J, Zhuo H, Zhang X, et al. A novel biomarker Linc00974 interacting with KRT19 promotes proliferation and metastasis in hepatocellular carcinoma. *Cell Death Dis* 2014;5:e1549.
- Yan J, Xie G, Liang C, et al. Herbal medicine Yinchenhaotang protects against a-naphthylisothiocyanate-induced cholestasis in rats. *Sci Rep* 7(1): 4211.
- Kaiser S, Gerok W, Haussinger D. Ammonia and glutamine metabolism in human liver slices: new aspects on the pathogenesis of hyperammonaemia in chronic liver disease. *Eur J Clin Invest* 1988;18(5):535–42.
- Ong JP, Aggarwal A, Krieger D, et al. Correlation between ammonia levels and the severity of hepatic encephalopathy. *Am J Med* 2003;114(3):188–93.
- Butterworth RF. Pathogenesis of hepatic encephalopathy: new insights from neuroimaging and molecular studies. *J Hepatol* 2003;39(2):278–85.
- Belanger M, Desjardins P, Chatauret N, Butterworth RF. Loss of expression of glial fibrillary acidic protein in acute hyperammonemia. *Neurochem Int* 2002;41(2–3): 155–60.
- Kril JJ, Butterworth RF. Diencephalic and cerebellar pathology in alcoholic and non-alcoholic patients with end-stage liver disease. *Hepatology* 1997;26(4):837–41.
- Hoyumpa Jr AM, Desmond PV, Avant GR, Roberts RK, Schenker S. Hepatic encephalopathy. *Gastroenterology* 1979;76(1):184–95.
- Guevara M, Baccaro ME, Gomez-Anson B, et al. Cerebral magnetic resonance imaging reveals marked abnormalities of brain tissue density in patients with cirrhosis without overt hepatic encephalopathy. *J Hepatol* 2011;55(3):564–73.
- Yang N, Liu H, Jiang Y, et al. Lactulose enhances neuroplasticity to improve cognitive function in early hepatic encephalopathy. *Neural Regen Res* 2015;10(9):1457–62.
- Miethke AG, Zhang W, Simmons J, et al. Pharmacological inhibition of apical sodium-dependent bile acid transporter changes bile composition and blocks progression of sclerosing cholangitis in multidrug resistance 2 knockout mice. *Hepatology* 2016;63(2):512–23.
- Baghdasaryan A, Fuchs CD, Osterreicher CH, et al. Inhibition of intestinal bile acid absorption improves cholestatic liver and bile duct injury in a mouse model of sclerosing cholangitis. *J Hepatol* 2016;64(3):674–81.
- Hiott DW, Labbate L. Anxiety disorders associated with traumatic brain injuries. *NeuroRehabilitation* 2002;17(4):345–55.
- Chauhan NB, Gatto R, Chauhan MB. Neuroanatomical correlation of behavioral deficits in the CCl model of TBI. *J Neurosci Methods* 2010;190(1):1–9.
- Fitz G. Systemic complications of liver disease. In: Feldman M, Scharschmidt BF, Sleisinger MH, editors. *Gastrointestinal and Liver Disease*. Philadelphia: Saunders Company; 1998. p. 1334–54.
- Zuidema GD, Sherman B, Cullen D, Kirsh MM. Effect of urease inhibition on ammonia intoxication in dogs. *Archives of surgery (Chicago, Ill)* 1964;196(8):303–7.
- Gropper S, Smith J. *Advanced Nutrition and Human Metabolism*. Belmont: Yolanda Cossico; 2013.
- Haussinger D, Kircheis G, Fischer R, Schliess F, Vom Dahl S. Hepatic encephalopathy in chronic liver disease: a clinical manifestation of astrocyte swelling and low-grade cerebral edema? *J Hepatol* 2000;32(6):1035–8.
- Warren KS. Ammonia toxicity and pH. *Nature* 1962;195:47–9.
- Swales JD, Papadimitriou M, Wrong OM. Observations upon ammonia absorption from the human ileum. *Gut* 1973;14(9):697–700.
- Carey MC, Small DM. Micelle formation by bile salts. Physical-chemical and thermodynamic considerations. *Arch Intern Med* 1972;130(4):506–27.
- Manautou JE, Campion SN, Aleksunes LM. 9.08 - Regulation of Hepatobiliary Transporters during Liver Injury. In: McQueen CA, editor. *Comprehensive Toxicology*. Second Edition. Oxford: Elsevier; 2010. p. 175–220.
- Rodrigues CM, Spellman SR, Sola S, et al. Neuroprotection by a bile acid in an acute stroke model in the rat. *Journal of Cerebral Blood Flow and Metabolism* 2002;22(4): 463–71.
- Rodrigues CM, Sola S, Nan Z, et al. Tauroursodeoxycholic acid reduces apoptosis and protects against neurological injury after acute hemorrhagic stroke in rats. *Proc Natl Acad Sci U S A* 2003;100(10):6087–92.
- Finlayson MH, Superville B. Distribution of cerebral lesions in acquired hepatocerebral degeneration. *Brain* 1981;104:79–95 Pt 1.
- Butterworth R. Neuronal cell death in hepatic encephalopathy. *Metab Brain Dis* 2007;22(3–4):309–20.
- Balzano T, Forteza J, Molina P, et al. The Cerebellum of patients with Steatohepatitis shows Lymphocyte Infiltration, Microglial Activation and loss of Purkinje and Granular Neurons. *Sci Rep* 2018;8(1):3004.
- Chiodini I, Adda G, Scillitani A, et al. Cortisol secretion in patients with type 2 diabetes: relationship with chronic complications. *Diabetes Care* 2007;30(1):83–8.
- Gong S, Miao YL, Jiao GZ, et al. Dynamics and correlation of serum cortisol and corticosterone under different physiological or stressful conditions in mice. *PLoS One* 2015;10(2):e0117503.
- Ocon B, Aranda CJ, Gamez-Belmonte R, et al. The glucocorticoid budesonide has protective and deleterious effects in experimental colitis in mice. *Biochem Pharmacol* 2016;116:73–88.
- Greenamyre JT, Sanders LH, Gasser T. Fruit flies, bile acids, and Parkinson disease: a mitochondrial connection? *Neurology* 2015;85(10):838–9.
- Weill-Engerer S, David JP, Szadovitch V, et al. Neurosteroid quantification in human brain regions: Comparison between Alzheimer's and nondemented patients. *J Clin Endocr Metab* 2002;87(11):5138–43.